CHEMISTRY OF MATERIALS

ARTICLE

pubs.acs.org/cm

Highly Stable Red Oxynitride β-SiAlON:Pr^{3+} Phosphor for Light-Emitting Diodes

Tzu-Chen Liu,[†] Bing-Ming Cheng,[‡] Shu-Fen Hu,[§] and Ru-Shi Liu[†,*]

[†]Department of Chemistry, National Taiwan University, Taipei 106, Taiwan

[‡]National Synchrotron Radiation Research Center, Hsinchu 300, Taiwan

[§]Department of Physics, National Taiwan Normal University, Taipei 116, Taiwan

Supporting Information

ABSTRACT: Trivalent Pr^{3+}-doped oxynitirde red phosphors β-SiAlON with composition $Si_{6-z}Al_zO_zN_{8-z}:Pr_x$ (z = 0−2.0, x = 0.016) were synthesized by gas pressure sintering (GPS) at 1950 °C for 2 h. Red luminescence in the range 600−650 nm was detected upon excitation with 460 nm blue light, indicating that the phosphor can be excited by blue InGaN light-emitting diodes (LED). The crystallization and cell parameters of samples were investigated by powder X-ray diffraction (XRD), Rietveld refinement, and high-resolution transmission electron microscopy (HRTEM). Energy-dispersive X-ray spectroscopy (EDX) and scanning electron microscopy (SEM) were further adopted to examine the effect of Al substitution on the microstructure. ^{27}Al and ^{29}Si solid-state nuclear magnetic resonance (NMR) data are consistent with $SiN_{4-x}O_x$ and partially substituted $AlN_{4-x}O_x$ tetrahedra. The temperature-dependent luminescence from the $^1D_2$ and $^3P_0$ states of Pr^{3+} were studied (10−573 K), and the integrated red emission from 600 to 650 nm increased with temperature (298−473 K). This unexpected phenomenon is proposed to be the result of two crossed excitation states in the configurational coordination diagram. This investigation reveals the superior characteristics of nitride compounds and the feasibility of doping Pr^{3+} into phosphor.

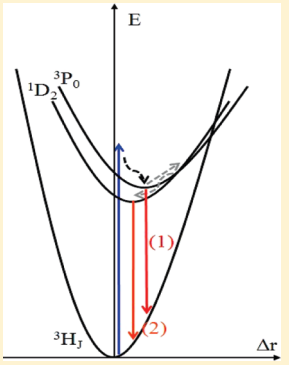

KEYWORDS: phosphor, blue LED, solid-state NMR, Pr^{3+}, thermal stability

INTRODUCTION

Silicon nitride is an important industrial material because of its excellent properties such as high strength, high chemical and thermal stabilities, and high decomposition temperature.[1−3] Recently, Si_3N_4-based derivatives have emerged as good candidates for rare-earth-doped phosphors because of their excellent optical properties upon excitation with ultraviolet (UV) or blue light.[4−6] Rigid nitride coordination around the rare earth ions has a strong nephelauxetic effect and crystal field splitting, which increase excitation and emission wavelengths.[7] Silicon nitride has two major crystalline phases, α and β. Both phases comprise corner-sharing SiN_4 tetrahedra with different stacking orders ABCDABCD for α-Si_3N_4 and ABAB for β-Si_3N_4. The CD layer in α-Si_3N_4 is the AB layer by a c-glide plane. Therefore, α-Si_3N_4 has a trigonal structure, and β-Si_3N_4 has a hexagonal structure. Both α and β-SiAlON phases have been chosen as host lattices, which can be described as $M_{m/v}Si_{12-(m+n)}Al_{m+n}O_nN_{16-n}$ and $Si_{6-z}Al_zO_zN_{8-z}$, respectively, where v is the valence of metal M and z is the number of Al−O bonds that are substituted by Si−N bonds and is in the range $0 < z \leq 4.2$.[8]

Compared with α-SiAlON, β-SiAlON has attractecd less attention. The ABCD stacking order causes α-SiAlON to have two interstitial sites per unit cell; M can be Li, Ca, Sr, Lu, Y, or one of a number of rare earth (RE) ions.[9−17] On the other hand, RE ions can reside only along the continuous [0001] channel at β-SiAlON, and no insertion of M has been possible until now.[18−20] In 1985, Popma et al. reported for the first time the luminescence properties of β-SiAlON;[21] however, they considered examples in which z = 3, which is obviously too high to retain a pure β-Si_3N_4 phase, according to recent studies.[22,23] The luminescence properties of β-SiAlON that is doped with Eu^{2+} and Ce^{3+} have been described. Phosphors such as yellow Ca-α-SiAlON:Eu^{2+}, green β-SiAlON:Eu^{2+}, and red $CaAlSiN_3$:Eu^{2+} have been combined, and SiAlON-based phosphors have thus been found to be thermally stable phosphors to increase the color rendering index (CRI).[24]

Among various rare earth ions, Pr^{3+} ions are particularly versatile. The luminescence of Pr^{3+} originates from three excited states, $^1S_0$, $^3P_0$, and $^1D_2$; it depends strongly on the host lattice and is in the range from UV to infrared.[22] The emission of β-SiAlON:Pr^{3+} originates mainly from the $^3P_0$ and $^1D_2$ states and is in the red region; the excitation of the $^3H_4 \rightarrow {}^3P_J$ transition situates at the blue region with the highest intensity at 460 nm. In the present study, we investigate the more detailed crystal structure, the photoluminescence properties of Pr^{3+}-doped β-SiAlON, the effect of Al/O substitution, and its unusual thermal quenching behaviors. The characteristics indicate that nitride or oxynitride phosphors can serve as good lattice hosts and Pr^{3+} ions can be used as red emitting ions.

Received: May 6, 2011
Revised: July 7, 2011
Published: July 22, 2011

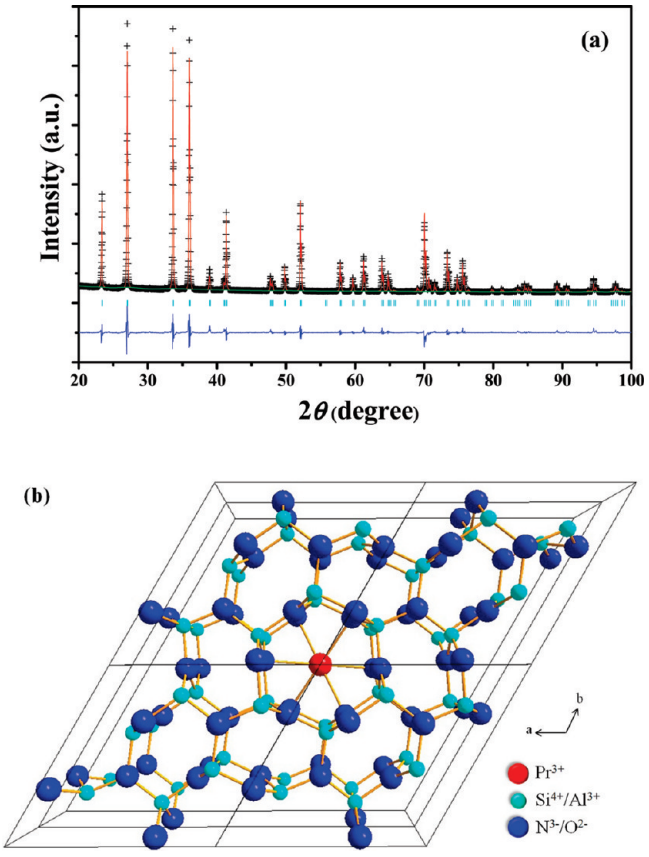

Figure 1. (a) Rietveld refinement of the powder XRD pattern of $Si_{5.9}Al_{0.1}O_{0.1}N_{7.9}:Pr_{0.016}$. Observed (crosses) and calculated (red line) XRD patterns. Cyan vertical lines indicate positions of Bragg reflections. Blue line represents difference plot (observed − calculated) on the same scale. (b) Crystal structure of 2 × 2 × 2 unit cells of $Si_{5.9}Al_{0.1}O_{0.1}N_{7.9}:Pr_{0.016}$ viewed in *c*-direction.

EXPERIMENTAL SECTION

Synthesis. $Si_{6-z}Al_zO_zN_{8-z}:Pr_x$ ($z = 0-2.0$, $x = 0.016$) were prepared from α-Si_3N_4 (Ube Industries, grade SN-E10, $\alpha/(\alpha+\beta) > 95\%$ by wt), AlN (Tokuyama Corp., type F), Al_2O_3 (Taimei Chemicals Co. Ltd., grade TM-DAR), and Pr_2O_3 (Cerac Inc., 99.9%, 325 mesh) as starting powders, using the GPS method. For each composition, a total of 1.5 g starting material was weighed and mixed by hand in an agate mortar according to different value of *z*. The powder mixtures were packed into boron nitride crucibles and then fired in the GPS furnace (FVPHP-R-5, FRET-25, Fujidempa Kogyo Co. Ltd.) with a graphite heater at a constant heating rate of 10 °C/min from room temperature to 1200 °C in a vacuum of 10^{-2} Pa. At 1200 °C, nitrogen (99.999% purity) was introduced to a pressure of 0.92 MPa. From 1200 to 1950 °C, the heating rate was reduced to 5 °C/min, and the temperature was maintained at 1600 °C for 3 h in between to make α phase transform to β phase completely. Finally, the samples were heated at 1950 °C for 2 h, and the heating power was turned off to make the cooling to room temperature within 3 h. The samples were ground into powder for subsequent analysis.

Characterization. The composition and phase purity of the samples were studied by XRD using a PANalytical XPert'Pert PRO with Cu Kα radiation ($\lambda = 1.5418$ Å) operated at 45 kV and 40 mA. The data were collected over a 2θ range from 20° to 100° at intervals of 0.02° with a counting time of 30 s per step. The crystal structure was refined by the Rietveld method using the General Structure Analysis System (GSAS) program.[25] The photoluminescence (PL) spectra were obtained using a FluoroMax-3 spectrophotometer at room temperature with a 150W Xe lamp and a Hamamatsu R928 photomultiplier tube (PMT). Time-resolved photoluminescence decays were recorded by a FluoroMax-4 time-correlated single-photon counting (TCSPC) spectrofluorometer using a interchangeable Nano LED source for excitation. The vacuum ultraviolet (VUV) PL and photoluminescent excitation (PLE) spectra were obtained at the National Synchrotron Radiation Research Center in Taiwan using a BL03A beamline. The PLE spectra were recorded by scanning a 6 m cylindrical grating monochromator with a grating of 450 grooves/mm, which spanned the wavelength range of 100−350 nm. A CaF_2 plate served as a filter to remove the high-order light from the synchrotron. The emission from the phosphor was analyzed with a 0.32 m monochromator and was detected in a photon-counting mode. Cooling to 10−298 K was achieved by liquid helium cooling. Thermal quenching was identified using a heating apparatus (THMS-600) in combination with PL equipment (298−573K). The particle size and morphology of the samples were examined using scanning electron microscopy (SEM; Hitachi S2400), and the element composition was determined using an energy-dispersive X-ray spectroscopy (EDX) that was attached to the SEM. The crystal structures were analyzed by high-resolution transmission electron microscopy (HRTEM; JEM-2000EX, operating at 200 kV)

Solid-state nuclear magnetic resonance (NMR) spectra were acquired on a Bruker DSX 300 MHz NMR spectrometer equipped with a 4 mm double-resonance magic-angle-spinning (MAS) probehead. The Larmor frequencies for ^{29}Si and ^{27}Al were 59.63 and 78.22 MHz, respectively. ^{29}Si single pulse experiments were carried out using a $\pi/3$ pulse (3 μs), a recycle delay of 60 s, and a sample spinning rate of 5 kHz. ^{27}Al signals were collected after a selective pulse ($<\pi/6$) of 3 μs with a recycle delay of 1 s and a spinning rate of 12 kHz. ^{29}Si and ^{27}Al chemical shifts were reported relative to external tetramethylsilane and 1 M aqueous $Al(NO_3)_3$, respectively.

Table 1. Structure Parameters of $Si_{5.9}Al_{0.1}O_{0.1}N_{7.9}:Pr_{0.016}$ as Determined by Rietveld Refinement of Power XRD Data at Room Temperature[a]

atom	site	*x*	*y*	*z*	occu.	*U* (Å^2)
Si1	6 h	0.17401(3)	0.76639(7)	0.25000(0)	0.9833	0.0321
Al1	6 h	0.17401(3)	0.76639(7)	0.25000(0)	0.0167	0.0321
N1	2c	0.33330(0)	0.66670(0)	0.25000(0)	0.9875	0.0386
O1	2c	0.33330(0)	0.66670(0)	0.25000(0)	0.0125	0.0386
N1	6 h	0.32893(7)	0.02770(2)	0.25000(0)	0.9875	0.0298
O1	6 h	0.32893(7)	0.02770(2)	0.25000(0)	0.0125	0.0298

[a] Space group: *P*63/*m* (No. 176), $Z = 2$, $V = 145.933(2)$ Å^3, $a = b = 7.60593(4)$ Å, $c = 2.91009(6)$ Å, $R_p = 7.47\%$, $R_{wp} = 10.72\%$, $\chi^2 = 3.26$.

RESULTS AND DISCUSSION

Crystal Structure. Panel (a) of Figure 1 shows the results of the Rietveld refinement of $Si_{5.9}Al_{0.1}O_{0.1}N_{7.9}:Pr_{0.016}$ with $\chi^2 = 3.26$. The black crosses and red line represent the observed and calculated patterns, respectively. The results ensure the purity of the sample phase. The compound has a hexagonal structure with the space group P63/m, and its cell parameters are $a = b = 7.60953(4)$ Å, $c = 2.91009(6)$ Å. Panel (b) of Figure 1 shows the 2 × 2 ×2 unit cells of β-SiAlON:Pr^{3+} viewed from [0001]. Si ions form SiN_4 tetrahedra, and they are joined by sharing corners in a way that N ions connect to three tetrahedra. The Pr^{3+} ion is assumed to be located at (0, 0, 0.5) and to be surrounded by six nitrogen ions and have a coordination number (CN) of 6.[26] The refinement process did not replace rare earth ions with any

dx.doi.org/10.1021/cm201289s |*Chem. Mater.* 2011, 23, 3698–3705

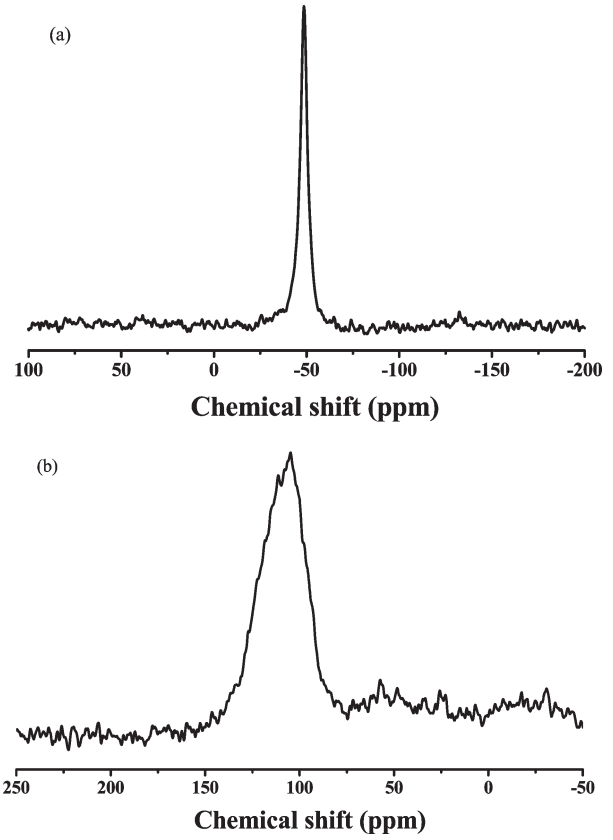

Figure 2. Solid-state NMR spectra of $Si_{5.9}Al_{0.1}O_{0.1}N_{7.9}:Pr_{0.016}$ for (a) ^{29}Si and (b) ^{27}Al.

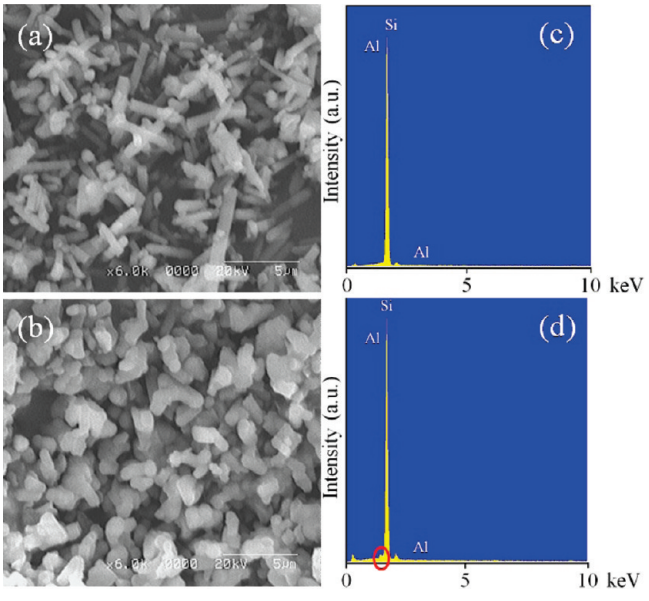

Figure 3. SEM images of $Si_{6-z}Al_zO_zN_{8-z}:Pr_{0.016}$ with z values of (a) 0 and (b) 0.1. EDX spectra of $Si_{6-z}Al_zO_zN_{8-z}:Pr_{0.016}$ with z values of (c) 0 and (d) 0.1.

elements in the host lattice if compared to a previous study[19] because we believe that the differences between the ionic sizes of the host elements and rare earth ions Si^{4+} (4CN, 0.26 Å), Al^{3+} (4CN, 0.39 Å), and Pr^{3+} (6CN, 0.99 Å) are too large.[27] During

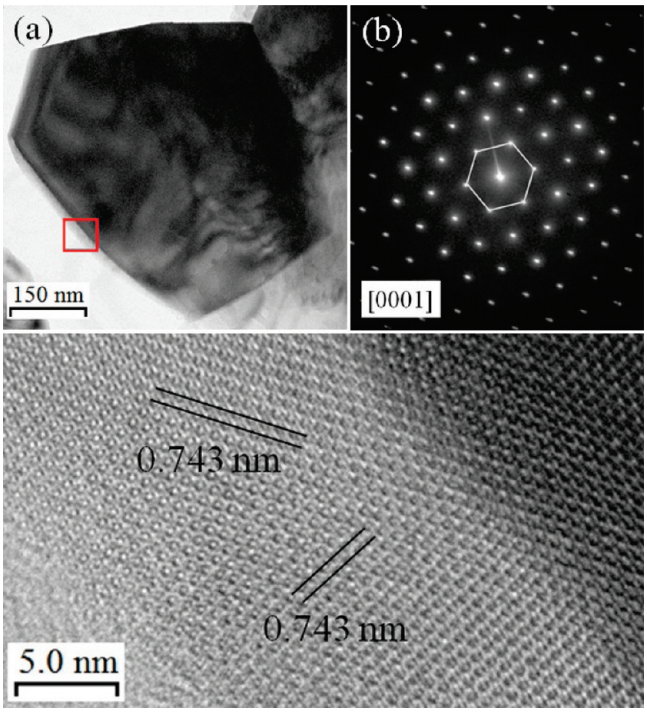

Figure 4. (a) TEM images of a $Si_{5.9}Al_{0.1}O_{0.1}N_{7.9}:Pr_{0.016}$, (b) corresponding SAED, and (c) HRTEM images of the selected area in panel (a).

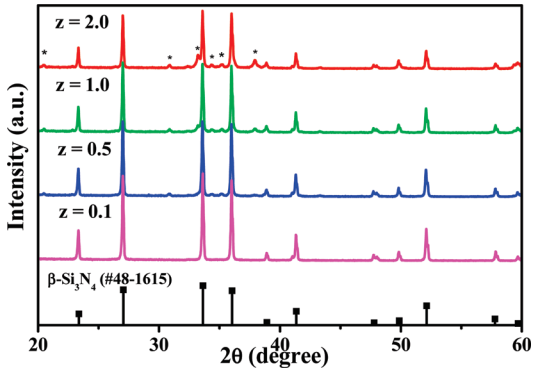

Figure 5. Powder XRD patterns of $Si_{6-z}Al_zO_zN_{8-z}:Pr_{0.016}$ with $z = 0.1$, 0.5, 1.0, and 2.0.

the refinement procedure, the occupancy parameters of all atoms were evaluated with reference to the nominal stoichiometry and verified very accurately by EDX measurement. The temperature factors were fixed for all substituted ions. Table 1 presents the structure parameters of $Si_{5.9}Al_{0.1}O_{0.1}N_{7.9}:Pr_{0.016}$.

Solid-state NMR can be used to study the substitution of Al/O to Si/N and their connection environment. In the β-Si_3N_4 crystal, because of the ABAB stacking order, only one equivalent silicon site is available. As panel (a) of Figure 2 shows, one peak at −48.6 ppm is observed, matching well with the value in the literature for 4-fold coordinated Si atoms. In contrast, α-Si_3N_4 has an average bond length difference of 0.021 Å and so yields two peaks at −49.0 and −47.1 ppm.[28] This result provides further confirmation that the transformation from α-Si_3N_4 to β-Si_3N_4 is complete when the temperature is held at 1600 °C for

dx.doi.org/10.1021/cm201289s |Chem. Mater. 2011, 23, 3698–3705

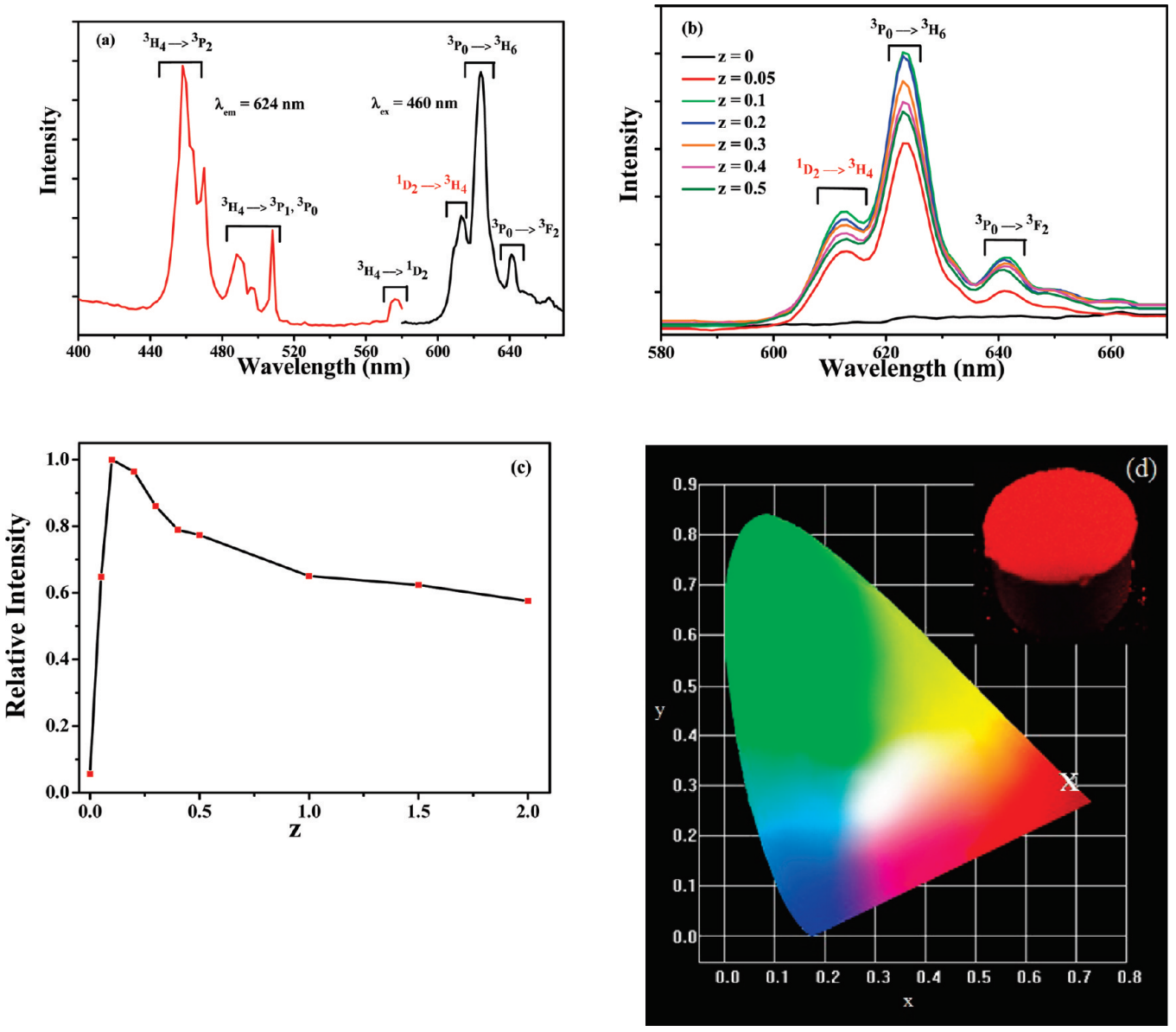

Figure 6. (a) Excitation (λ_{em} = 624 nm) and emission spectra (λ_{ex} = 460 nm) of $Si_{5.9}Al_{0.1}O_{0.1}N_{7.9}$:$Pr_{0.016}$. (b) Comparison of emission spectra at different z values. (c) Effect of Al and O substitution on luminescent properties of $Si_{6-z}Al_zO_zN_{8-z}$:$Pr_{0.016}$. (d) CIE chromaticity coordinates of $Si_{6-z}Al_zO_zN_{8-z}$:$Pr_{0.016}$ in wavelength range 600−650 nm. Inset shows photograph of $Si_{6-z}Al_zO_zN_{8-z}$:$Pr_{0.016}$ irradiated under 254 nm UV lamp box.

3 h under a nitrogen pressure of 0.92 MPa. In the β-SiAlON host, Al atoms are surrounded by N with a portion of O because charge compensation requires that at least one of the nearest neighbors to Al is O. Panel (b) of Figure 2 demonstrates the measured ^{27}Al spectrum with one peak at 104.9 ppm close to the value in the literature.[29] Doping with a trace amount of Pr^{3+} ions does not have a strong effect on the solid-state NMR data.

The morphology of β-SiAlON is of importance because the hexagonal crystal structure tends to grow along the c-axis to form rod-like crystals. This process is disadvantageous when mixing with other round phosphors.[30] Therefore, the effect of Al incorporation is examined by SEM and confirmed by EDX. Panels (a) and (c) of Figure 3 display the SEM image of $Si_{6-z}Al_zO_zN_{8-z}$:$Pr_{0.016}$ with z = 0 and the corresponding EDX spectrum. The products have a uniform rod-like shape with a length of approximately 3 μm and a diameter of 0.5 μm. When a small amount of Al was added as shown in panel (b) of Figure 3, the crystals become spherical with a diameter of around 0.5 μm, suggesting that the incorporation of Al contributes to the increased amount of transient liquid phases that accelerate the dissolution, diffusion, and precipitation processes for crystal growth.[31] The EDX spectrum in panel (d) of Figure 3 further verifies that Al was successfully incorporated into the crystal as circled at 1.5 keV, and panel (c) of Figure 3 includes no Al signal. The amounts of Al, z = 0−2.0, detected by EDX are summarized in the Table S1 of the Supporting Information. Panel (a) of Figure 4 presents the fine structure of the $Si_{5.9}Al_{0.1}O_{0.1}N_{7.9}$:$Pr_{0.016}$ crystal identified using HRTEM. The selected area electron diffraction pattern (SAED) taken from the sample is shown in panel (b) of Figure 4, and one set of the regular hexagon diffraction pattern was observed, indicating that the product has a hexagonal crystal structure. Panel (c) of Figure 4 is the HRTEM

dx.doi.org/10.1021/cm201289s |*Chem. Mater.* 2011, 23, 3698–3705

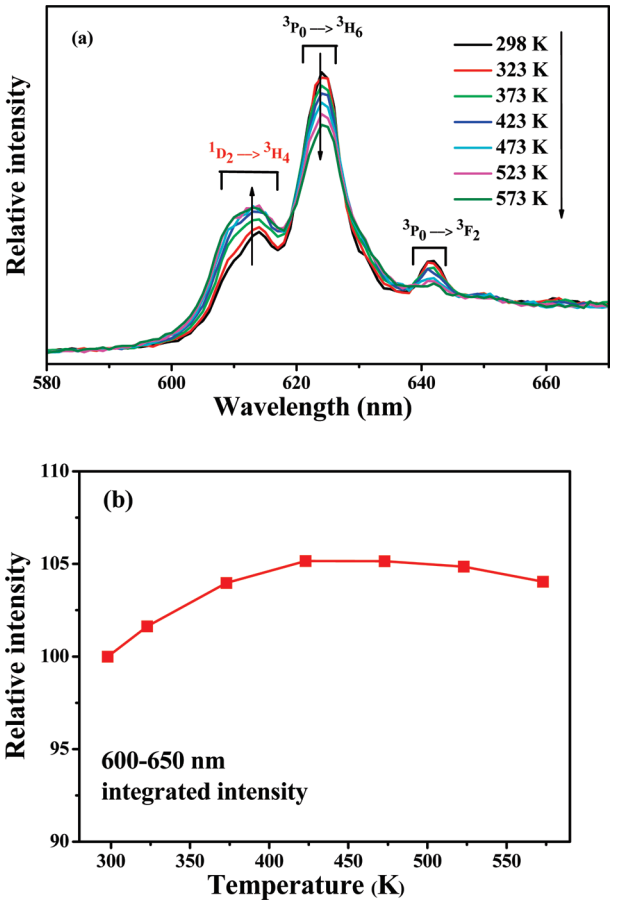

Figure 7. (a) Temperature-dependent emission spectra of $Si_{5.9}Al_{0.1}O_{0.1}N_{7.9}:Pr_{0.016}$ from 298 to 573 K. (b) Integrated emission intensities from 600−650 nm at different temperature.

image of the selected area in panel (a) of Figure 4. The TEM image and SAED reveal that the samples are single crystalline and the *c*-direction is perpendicular to the sample. The interplanar distance of 7.43 Å matches well with the refined value.

The amount of Al/O incorporation also influences the purity of the β-SiAlON phase. Figure 5 plots the phase transformation for increasing *z*. Transformations at values of $z = 0.1$, 0.5, 1.0, and 2.0 only are shown for clarity. Asterisks at $2\theta = 20.5$, 30.9, 33.2, 34.4, 35.2, and 37.9 are the mixed phases of α-Si_3N_4, AlN, and Al_2O_3. Impure phases emerge at $z = 0.3-0.4$, but they become obvious when *z* exceeds 1. XRD data of $Si_{6-z}Al_zO_zN_{8-z}:Pr_{0.016}$ with $z = 0-2.0$ are drawn in Figure S1 of the Supporting Information. The appearance of α-Si_3N_4 suggests that tolerance for the incorporation of Al/O is not high when the β-SiAlON host is doped with Pr^{3+} ions. In this work, no SiAlON polytypoid phases are observed. Compared with previous studies, in which increasing *z* gave rise to polytypoid phases upon doping with Eu^{2+} but not with Ce^{3+}.[32,33] This finding may be the result of ionic size disparities among Pr^{3+} (6CN, 0.99 Å), Ce^{3+} (6CN, 1.01 Å), and Eu^{2+} (6CN, 1.17 Å).[27]

Luminescence Properties. Panel (a) of Figure 6 displays the excitation and emission spectra of $Si_{5.9}Al_{0.1}O_{0.1}N_{7.9}:Pr_{0.016}$ at room temperature. The phosphor exhibits several sharp emission lines in the range 600−650 nm. Under 460 nm excitation, three narrow emission peaks are obtained at 613, 624, and 641 nm corresponding to the $^1D_2 \rightarrow {}^3H_4$, $^3P_0 \rightarrow {}^3H_6$, and $^3P_0 \rightarrow {}^3F_2$ transitions of Pr^{3+} ions, respectively. Greenish-blue emissions from $^3P_0$ to $^3H_4$ and $^3H_5$ are weak as panel (d) of Figure 6 shows the photograph of $Si_{5.9}Al_{0.1}O_{0.1}N_{7.9}:Pr_{0.016}$ under 254 nm excitation and its Commission International de I'Eclairage (CIE) chromaticity coordinate within the red region 600−650 nm. The excitation spectrum monitoring 624 nm consists of five excitation peaks, which can be grouped as 460/470 nm, 488/498 nm, and 509 nm, corresponding to the $^3H_4 \rightarrow {}^3P_J$ ($J = 2, 1, 0$) transitions, respectively. Because the six nitrogen ions around the Pr^{3+} center are randomly substituted by oxygen ions, oxygen replacement is reasonably assumed to cause Stark splitting by the altered matrix crystal field.[34] The splitting is estimated to be about 450 cm^{-1}. The peak at 578 nm is the $^3H_4 \rightarrow {}^1D_2$ transition and will be discussed later.

The incorporation of Al/O affects not only phase purity but also the luminescence properties as panel (b) of Figure 6 demonstrates the indispensable effect of adding Al/O to the β-Si_3N_4 host lattice. When Pr^{3+} ions were doped into the β-Si_3N_4 host lattice (here it should not be written as β-SiAlON), the phosphor $Si_{6-z}Al_zO_zN_{8-z}:Pr_{0.016}$ with $z = 0$ emits negligible intensity. The dependence of the emission of light by activators on Al/O substitution remains unclear, and the example presented herein is the first demonstration of the neglibible intensity from β-SiAlON:RE with $z = 0$. When the *z* value is increased to 0.05, the emission intensity of $Si_{5.95}Al_{0.05}O_{0.05}N_{7.95}:Pr_{0.016}$ is around 65% of that with $z = 0.1$. The dependence of the emission intensity and *z* values is shown in panel (c) of Figure 6, where $Si_{5.9}Al_{0.1}O_{0.1}N_{7.9}:Pr_{0.016}$ has highest intensity, and it decreases monotonically with increasing *z*.

Thermal stability is a critical property of phosphor-converted light emitting diodes (pc-LEDs) because high-power LEDs can reach 450 K. Panel (a) of Figure 7 shows the temperature dependence of the emission spectra of Pr^{3+}-doped β-SiAlON; emission intensity at 613 nm from the $^1D_2 \rightarrow {}^3H_4$ transition increases with temperature to 523 K. To verify this unusual behavior, Pr^{3+}-doped β-SiAlON with different *z* values and different Pr^{3+} concentration have been measured, and they showed similar results (data not shown). Emission peaks from the $^3P_0$ state all decrease with increasing temperature. These include those from $^3P_0 \rightarrow {}^3F_2$ at 641 nm and less intense $^3P_0$ to $^3H_4$ and $^3H_5$ transitions, as shown in Figure S2 of the Supporting Information. Because of the unexpected increase in the 613 nm peak, panel (b) of Figure 7 shows the integrated area in the range 600−650 nm, which also increases to 423 K. It is worth noting that in order to maintain good color quality in display panel, it is better for the CIE chromaticity coordinate to have a smaller shift upon increasing temperature. When phosphors are doped with Eu^{2+} and Ce^{3+} activators, which emit light from 5d → 4f transition, they are likely to have large blue shift or red shift with increasing temperature because the 5d energy level has a greater tendency to be affected by the crystal field.[35,36] Because 4f electrons of Pr^{3+} ions are surrounded by 5s and 5p electrons, the peak positions hardly change. The increase of 613 nm and decrease of 624 and 641 nm make the CIE chromaticity coordinates shift to lower *x* and higher *y*; β-SiAlON:Pr^{3+} therefore only shifts from (0.6876, 0.3122) at 298 K to (0.6851, 0.3148) at 573 K. The CIE chromaticity coordinates with different temperatures are presented in Table S2 of the Supporting Information.

The presence of $^3H_4 \rightarrow {}^3P_J$ ($J = 2, 1, 0$) peaks in the excitation spectrum clearly indicates that a nonradiative relaxation from $^3P_0 \rightarrow {}^1D_2$ happens. To investigate the mechanism of this process, it

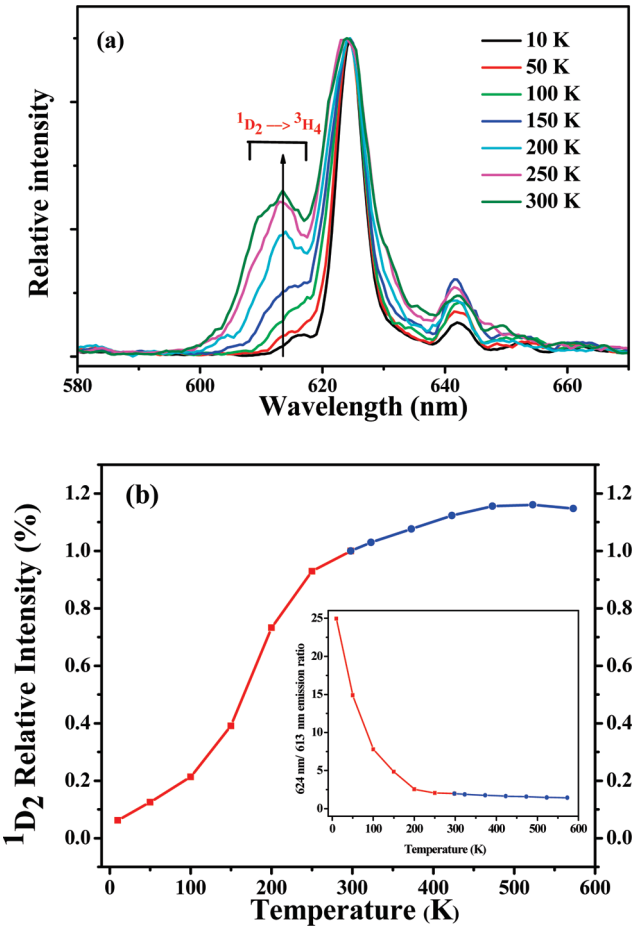

Figure 8. (a) Temperature-dependent emission spectra of $Si_{5.9}Al_{0.1}O_{0.1}N_{7.9}:Pr_{0.016}$ from 10 to 298 K (b) Temperature-dependent emission intensities for the $^1D_2 \rightarrow {}^3H_4$ transition from 10 to 573 K. Inset shows ratio of emission intensities from the $^3P_0$ and $^1D_2$ states.

is investigated at low temperature. Figure S3 of the Supporting Information presents the low-temperature excitation spectrum monitored at 624 nm. The 4f5d → $4f^2$ transition and the host lattice contribute to the broad band excitation spectrum. The Pr^{3+} emission under broad band excitation is the same as under $^3H_4 \rightarrow {}^3P_2$ excitation, as panel (a) of Figure 8 demonstrates the emission spectra of $Si_{5.9}Al_{0.1}O_{0.1}N_{7.9}:Pr_{0.016}$ from 10 to 298 K. The $^1D_2$ emission line is absent at 10 K and gradually increases with increasing temperature. For clarity, only $^1D_2 \rightarrow {}^3H_4$ and $^3P_0 \rightarrow {}^3H_6$ transitions are compared here, with the intensities of the latter one normalized. Combined with previous data, panel (b) of Figure 8 plots the temperature-dependent emission intensity diagram of the $^1D_2 \rightarrow {}^3H_4$ transition from 10 to 573 K. The emission value at 298 K is set to be one, and the inset plots the ratio of emission at 624 nm to that at 613 nm. The intensities were compared on the basis of the maximum counts detected from PMT rather than the integrated area because the two transitions overlap each other. Table 2 presents the ratio of emission intensities with various temperatures.

Analysis of the luminescence decay curves is adopted to confirm the assignment of each peak because emission originating from the $^1D_2$ state has a longer lifetime than that of $^3P_0$.[37] Panels (a)−(e) of Figure 9 demonstrate the decay curves of the five detected emissions: 510, 528, 613, 624, and 641 nm, which

Table 2. Relative Intensities of Signals at 613 nm and Ratios of Intensities at 624 and 613 nm at Various Temperature

	613 nm $^1D_2 \rightarrow {}^3H_4$ relative intensity	624 and 613 nm ratio
10 K	0.06	25.00
50 K	0.13	14.89
100 K	0.21	7.79
150 K	0.39	4.85
200 K	0.73	2.55
250 K	0.93	2.06
298 K	1.00	1.97/1.97[a]
323 K	1.03	1.88
373 K	1.08	1.75
423 K	1.12	1.64
473 K	1.16	1.58
523 K	1.16	1.48
573 K	1.15	1.45

[a] The 624 and 613 nm ratio at 298 K from 285 and 460 nm excitation is 1.974 and 1.965, respectively.

correspond to $^3P_0 \rightarrow {}^3H_4$, $^3P_0 \rightarrow {}^3H_5$, $^1D_2 \rightarrow {}^3H_4$, $^3P_0 \rightarrow {}^3H_6$, and $^3P_0 \rightarrow {}^3F_2$ transitions, respectively. Lifetimes originate from the $^3P_0$ state ($^3P_0 \rightarrow {}^3H_{4,5}$ and $^3F_2$) are shorter than that of $^1D_2$. It should be mentioned that the lifetime of 624 nm has been affected by the lifetime of 613 nm owing to the extensive overlap between these two peaks. Single-exponential decay curves are observed for 510 and 528 nm. Temperature-dependent lifetime measurement will be published elsewhere.

Proposed Mechanisms. On the basis of the photoluminescence properties, the unexpected Pr^{3+} emission behaviors are now discussed. As mentioned above, the red emission from Pr^{3+} ions originates from $^1D_2$ and $^3P_0$ states, and the ratio between the intensities of these emissions is determined by a nonradiative relaxation process. Several de-excitation pathways have been proposed. They include (a) multiphonon relaxation,[38] (b) cross relaxation,[39] and (c) intervalence charge transfer state (IVCT) between Pr^{3+} and metal ions.[40] The energy-gap law for estimating the rate of multiphonon relaxation is given by

$$W_{NR}(T = 0\,K) = \beta_{el}\exp[-\alpha(\Delta E - 2\hbar\omega_{max})]$$

where $\beta_{el} = 10^7\ s^{-1}$ and $\alpha = 4.5(\pm 1) \times 10^{-3}$ cm. The number of phonons required to bridge the energy gap can be divided into two groups, which are 6−7 and fewer than six.[41] In the former case, hardly any light is emitted from the $^1D_2$ state, while in the second group, significant light can be emitted. In β-SiAlON:Pr^{3+}, the energy gap between the $^1D_2$ and $^3P_0$ states determined from the excitation spectrum is 2345 cm^{-1}, and the phonon energy is around 886 cm^{-1} (110 meV).[42] Therefore, 2.6 phonons are required to bridge the gap; the result is reasonable given the observed $^1D_2 \rightarrow {}^3H_4$ transition in this study. Cross relaxation occurs when the energy from excited states promote the ground state to the metastable level. In trivalent praseodymium, this process occurs between ($^3P_0$, $^3H_4 \rightarrow {}^1D_2$, $^3H_6$), ($^3P_0$, $^3H_4 \rightarrow {}^1G_4$, $^3H_6$), and ($^1D_2$, $^3H_4 \rightarrow {}^1G_4$, $^3F_4$). Other possibilities exist, and some of them increase the $^1D_2$ intensity, while others reduce it. However, this process is host-dependent and cannot explain the increase in $^1D_2$ intensity from 10 to 473 K and the subsequent decrease in this study. The intervalence charge transfer state, on the other hand, proposes a low-lying Pr-to-metal IVCT state that

dx.doi.org/10.1021/cm201289s |Chem. Mater. 2011, 23, 3698–3705

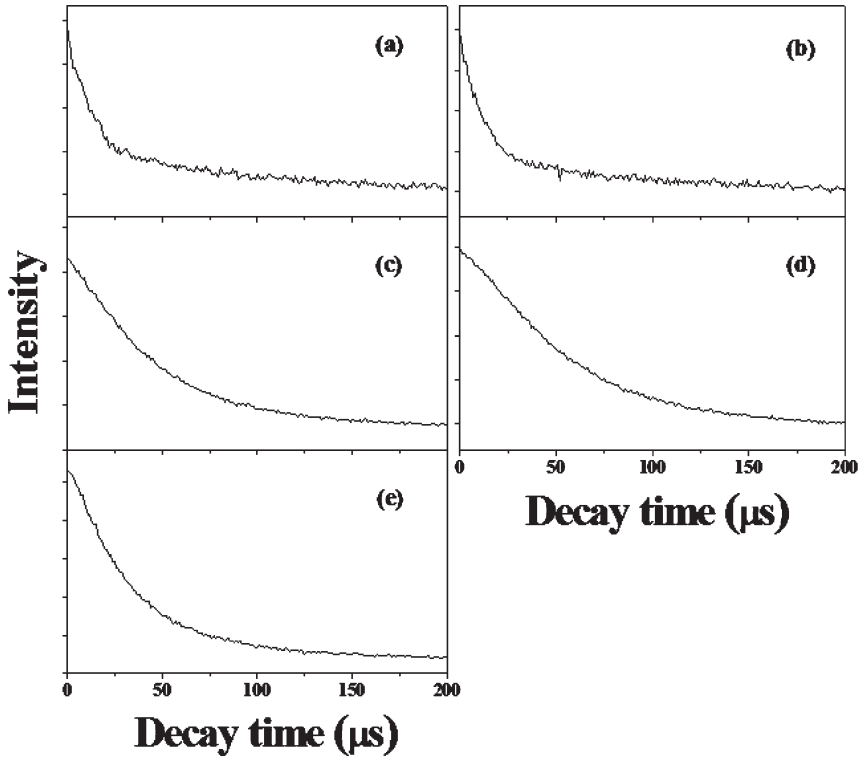

Figure 9. Decay curves of $Si_{6-z}Al_zO_zN_{8-z}:Pr_{0.016}$ excited by 460 nm, monitored at (a) 510 nm, (b) 528 nm, (c) 613 nm, (d) 624 nm, and (e) 641 nm.

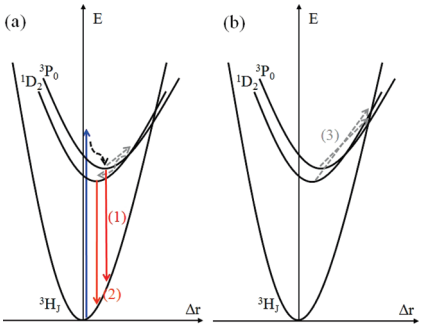

Figure 10. (a) and (b) Schematic configurational coordinate diagrams that present possible mechanisms of temperature-dependent emission of Pr^{3+} in the β-SiAlON host from the $^3P_0$ and $^1D_2$ states. For clarity, only $^3P_0$, $^1D_2$, and ^3H_J states are shown.

helps quench $^3P_0$ emission; nevertheless, the model focuses on oxide and transition metals, which is quite different to our case.[43]

The aforementioned pathways partly support the data but do not fully explain the observed behavior. To account for the characteristics of Pr^{3+} emission in β-SiAlON, we tentatively propose a model of two crossed excitation states, or a three parabola scheme,[44] depicted in Figure 10. In panel (a) of Figure 10, following the 460 nm excitation, electrons first relax to the equilibrium configuration of the $^3P_0$ state through vibrational relaxation. From this level, the system returns to the ground state and emits a 624 nm red line via (1); this process dominates at low temperature. As the temperature subsequently rises, thermal activation causes the electrons to cross the point of intersection of the $^3P_0$ and $^1D_2$ curves; thereby a 613 nm orange-red line is emitted via (2). This model successfully explains why the intensity of the the 624 nm signal declines monotonically as the temperature increases from 10 to 473 K and why the intensity of the 613 nm line increases. Panel (b) of Figure 10 demonstrates that thermal activation through (3) dominates when the temperature further increases over 473 K and explains why emissions from the $^3P_0$ and $^1D_2$ states are both quenched.

CONCLUSIONS

In summary, the Pr^{3+}-doped β-SiAlON red phosphor was synthesized by gas pressure sintering under 1950 °C for 2 h. The crystal structures were investigated by XRD, Rietveld refinement, and TEM in detail. The effect of Al/O substitution on the phosphor morphology was observed by SEM/EDX and verified by solid-state NMR ^{29}Si and ^{27}Al data. The photoluminescence properties of Pr^{3+} ions in the β-SiAlON host lattice were measured. The excitation spectra of β-SiAlON:Pr^{3+} with a broad band in the VUV region and several sharp lines in the 440−520 region could be excited by Xe atoms and InGaN blue LED chips, respectively. The intensity of the unexpected temperature-dependent luminescence behavior (10−573 K) at 613 nm, corresponding to the $^1D_2 \rightarrow {}^3H_4$ transition, increases with temperature and that at 624 nm from the $^3P_0 \rightarrow {}^3H_6$ transition decreases. An explanatory three parabola scheme was proposed. The emission intensity of 624 nm at 300 °C remains at 84% of that measured at room temperature. The high thermal stability reveals that β-SiAlON is a good candidate for wLEDs and Pr^{3+} is an alternative for red-emitting activators.

ASSOCIATED CONTENT

Supporting Information. Tables S1 and S2 and Figures S1, S2, and S3 show the amount of Si detected by EDX, CIE chromaticity coordinates with different temperature, XRD of

dx.doi.org/10.1021/cm201289s |Chem. Mater. 2011, 23, 3698–3705

$Si_{6-z}Al_zO_zN_{8-z}:Pr_{0.016}$ (z = 0−2.0), temperature-dependent emission spectra from $^3P_0$ to $^3H_4$ and $^3H_5$, and VUV excitation spectrum of $Si_{5.9}Al_{0.1}O_{0.1}N_{7.9}:Pr_{0.016}$, respectively. This material is available free of charge via the Internet at http://pubs.acs.org.

AUTHOR INFORMATION

Corresponding Author

*E-mail: rsliu@ntu.edu.tw.

ACKNOWLEDGMENT

The authors thank the National Science Council of the Republic of China, Taiwan, (Contracts NSC 97-2113-M-002-012-MY3 and NSC 97-3114-M-002) and the Everlight Electronics Co., Ltd. Taiwan, for financially supporting this research.

REFERENCES

(1) Jack, K. H. *J. Mater. Sci.* **1976**, *11*, 1135.
(2) Wang, C. M.; Pan, X. Q.; Ruhle, M.; Riley, F. L.; Mitomo, M. *J. Mater. Sci.* **1996**, *31*, 5281.
(3) Riley, F. L. *J. Am. Ceram. Soc.* **2000**, *83*, 245.
(4) Xie, R. J.; Hirosaki, N. *Sci. Technol. Adv. Mater.* **2007**, *8*, 588.
(5) Xie, R. J.; Hirosaki, N.; Sakuma, K.; Kimura, N. *J. Phys. D: Appl. Phys.* **2008**, *41*, 5.
(6) Xie, R. J.; Hirosaki, N.; Kimura, N.; Sakuma, K.; Mitomo, M. *Appli. Phys. Lett.* **2007**, *90*, 3.
(7) van Krevel, J. W. H.; Hintzen, H. T.; Metselaar, R.; Meijerink, A. *J. Alloys Compd.* **1998**, *268*, 272.
(8) Hampshire, S.; Park, H. K.; Thompson, D. P.; Jack, K. H. *Nature* **1978**, *274*, 880.
(9) Xie, R. J.; Hirosaki, N.; Mitomo, M.; Yamamoto, Y.; Suehiro, T.; Sakuma, K. *J. Phys. Chem. B* **2004**, *108*, 12027.
(10) Xie, R. J.; Hirosaki, N.; Mitomo, M.; Yamamoto, Y.; Suehiro, T.; Ohashi, N. *J. Am. Ceram. Soc.* **2004**, *87*, 1368.
(11) Xie, R. J.; Hirosaki, N.; Mitomo, M.; Uheda, K.; Suehiro, T.; Xu, X.; Yamamoto, Y.; Sekiguchi, T. *J. Phys. Chem. B* **2005**, *109*, 9490.
(12) Suehiro, T.; Hirosaki, N.; Xie, R. J.; Mitomo, M. *Chem. Mater.* **2005**, *17*, 308.
(13) Xie, R. J.; Hirosaki, N.; Mitomo, M.; Sakuma, K.; Kimura, N. *Appl. Phys. Lett.* **2006**, *89*, 3.
(14) Chan, T. S.; Lin, C. C.; Liu, R. S.; Xie, R. J.; Hirosaki, N.; Cheng, B. M. *J. Electrochem. Soc.* **2009**, *156*, J189.
(15) Li, Y. Q.; Hirosaki, N.; Xie, R. J.; Li, J.; Takeda, T.; Yamamoto, Y.; Mitomo, M. *J. Am. Ceram. Soc.* **2009**, *92*, 2738.
(16) Shioi, K.; Hirosaki, N.; Xie, R. J.; Takeda, T.; Li, Y. Q. *J. Mater. Sci.* **2010**, *45*, 3198.
(17) Suehiro, T.; Onuma, H.; Hirosaki, N.; Xie, R. J.; Sato, T.; Miyamoto, A. *J. Phys. Chem. C* **2010**, *114*, 1337.
(18) Hirosaki, N.; Xie, R. J.; Kimoto, K.; Sekiguchi, T.; Yamamoto, Y.; Suehiro, T.; Mitomo, M. *Appl. Phys. Lett.* **2005**, *86*, 3.
(19) Li, Y. Q.; Hirosaki, N.; Xie, R. J.; Takeda, T.; Mitomo, M. *J. Solid State Chem.* **2008**, *181*, 3200.
(20) Ryu, J. H.; Won, H. S.; Park, Y. G.; Kim, S. H.; Song, W. Y.; Suzuki, H.; Yoon, C. B.; Kim, D. H.; Park, W. J.; Yoon, C. *Electrochem. Solid State Lett.* **2010**, *13*, H30.
(21) Popma, T. J. European Patent, EP0155047A1, 1985.
(22) Ryu, J. H.; Park, Y. G.; Won, H. S.; Kim, S. H.; Suzuki, H.; Yoon, C. *J. Cryst. Growth* **2009**, *311*, 878.
(23) Zhu, X. W.; Masubuchi, Y.; Motohashi, T.; Kikkawa, S. *J. Alloys Compd.* **2010**, *489*, 157.
(24) Kimura, N.; Sakuma, K.; Hirafune, S.; Asano, K.; Hirosaki, N.; Xie, R. J. *Appl. Phys. Lett.* **2007**, *90*, 051109.
(25) Larson, C. Von Dreele, R. B. *Generalized Structure Analysis System (GSAS)*; Los Alamos National Laboratory Report LAUR 86-748; Los Alamos National Laboratory: Los Alamos, NM, 1994.
(26) Kimoto, K.; Xie, R. J.; Matsui, Y.; Ishizuka, K.; Hirosaki, N. *Appl. Phys. Lett.* **2009**, *94*, 041908.
(27) Shannon, R. D. *Acta Crystallogr., Sect. A* **1976**, *32*, 751.
(28) Dupree, R.; Lewis, M. H.; Lengward, G.; Williams, D. S. *J. Mater. Sci. Lett.* **1985**, *4*, 393.
(29) Mackenzie, K. J. D.; Smith, M. E. *Multinuclear Solid-State NMR of Inorganic Solids*; Pergamon: Amsterdam, 2002.
(30) Hirosaki, N. U.S. Patent, US2007108896A1, 1996.
(31) Xie, R. J.; Mitomo, M.; Xu, F. F.; Uheda, K.; Bando, Y. *Z. Metallkd.* **2001**, *92*, 931.
(32) Xie, R. J.; Hirosaki, N.; Li, H. L.; Li, Y. Q.; Mitomo, M. *J. Electrochem. Soc.* **2007**, *154*, J314.
(33) Liu, L. H.; Xie, R. J.; Hirosaki, N.; Takeda, T.; Zhang, C. N.; Li, J. G.; Sun, X. D. *J. Electrochem. Soc.* **2010**, *157*, H50.
(34) Savoini, B.; Santiuste, J. E. M.; Gonzalez, R. *Phys. Rev. B* **1997**, *56*, 585.
(35) Piao, X.; Horikawa, T.; Hanzawa, H.; Machida, K. *Appl. Phys. Lett.* **2006**, *88*, 161908.
(36) Li, Y. Q.; Hirosaki, N.; Xie, R. J.; Takeda, T.; Mitomo, M. *Chem. Mater.* **2008**, *20*, 6704.
(37) Huang, Y.; Tsuboi, T.; Seo, H. J. *J. Phys. Chem. A* **2008**, *112*, 5839.
(38) Vandijk, J. M. F.; Schuurmans, M. F. H. *J. Chem. Phys.* **1983**, *78*, 5317.
(39) Sokolska, I.; Golab, S.; Baluka, M.; Ryba-Romanowski, W. *J. Lumin.* **2000**, *91*, 79.
(40) Boutinaud, P.; Pinel, E.; Oubaha, M.; Mahiou, R.; Cavalli, E.; Bettinelli, M. *Opt. Mater.* **2006**, *28*, 9.
(41) Donega, C. D.; Meijerink, A.; Blasse, G. *J. Phys. Chem. Solids* **1995**, *56*, 673.
(42) Loong, C. K.; Richardson, J. W.; Sukuzi, S.; Ozawa, M. *J. Am. Ceram. Soc.* **1996**, *79*, 3250.
(43) Boutinaud, P.; Mahiou, R.; Cavalli, E.; Bettinelli, M. *Chem. Phys. Lett.* **2006**, *418*, 185.
(44) Di Bartolo, B. *Radiationless Processes*; Springer: Berlin, 1981.